Article

Chinese Science Bulletin

Geography

May 2011 Vol.57 No.14: 1716–1722
doi: 10.1007/s11434-012-5016-3

Evaluating cellulose absorption index (CAI) for non-photosynthetic biomass estimation in the desert steppe of Inner Mongolia

REN HongRui[1,2], ZHOU GuangSheng[1,3*], ZHANG Feng[1] & ZHANG XinShi[1*]

[1] *State Key Laboratory of Vegetation and Environmental Change, Institute of Botany, Chinese Academy of Sciences, Beijing 100093, China;*
[2] *Graduate University of Chinese Academy of Sciences, Beijing 100049, China;*
[3] *Chinese Academy of Meteorological Sciences, Beijing 100081, China*

Received September 20, 2011; accepted November 18, 2011; published online March 8, 2012

Accurate estimation of non-photosynthetic biomass is critical for modeling carbon dynamics within grassland ecosystems. We evaluated the cellulose absorption index (CAI), widely used for monitoring non-photosynthetic vegetation coverage, for non-photosynthetic biomass estimation. Our analysis was based on *in situ* hyperspectral measurements, during the growing seasons of 2009 and 2010, in the desert steppe of Inner Mongolia. ASD (Analytical Spectral Device)-derived and Hyperion-derived CAI were found to be effective for non-photosynthetic biomass estimation, yielding relative error (RE) values of 26.4% and 26.6%, respectively. The combination of MODIS (Moderate Resolution Imaging Spectroradiometer)-derived ($MODIS_2$–$MODIS_5$)/($MODIS_2$+$MODIS_5$) and ($MODIS_6$–$MODIS_7$)/($MODIS_6$+$MODIS_7$) showed a high multiple correlation (multiple correlation coefficient, r= 0.884) with ASD-derived CAI. A predictive model involving the two MODIS indices gave greater accuracy (RE=28.9%) than the TM (Landsat Thematic Mapper)-derived indices. The latter were the normalized difference index (NDI), the soil adjusted corn residue index (SACRI), and the modified soil adjusted crop residue index (MSACRI). These indices yielded RE values of more than 42%. Our conclusions have great significance for the estimation of regional non-photosynthetic biomass in grasslands, based on remotely sensed data.

non-photosynthetic vegetation, biomass, MODIS, TM, Hyperion, cellulose absorption index

Citation: Ren H R, Zhou G S, Zhang F, et al. Evaluating cellulose absorption index (CAI) for non-photosynthetic biomass estimation in the desert steppe of Inner Mongolia. Chin Sci Bull, 2012, 57: 1716–1722, doi: 10.1007/s11434-012-5016-3

In recent years, the terrestrial carbon cycle has received considerable attention by researchers and studies of its effect on global warming and other climatic and environmental issues have been at the frontier of earth science research [1]. Estimating size and dynamics of biomass has been one of the key issues for studies of the terrestrial carbon cycle [2]. Grasslands are one of the most widespread ecosystem types, and accurate assessment of grassland biomass is increasingly needed to reduce uncertainty about this terrestrial carbon sink [3,4]. Non-photosynthetic vegetation is an important component of grassland vegetation, and the amount of non-photosynthetic biomass is important in estimating carbon storage within grassland ecosystems. Traditional methods of biomass estimation are based on destructive sampling that is expensive and time-consuming. Remote sensing techniques offer a cost-effective solution for quantitative estimation of biomass from local to regional scales. During the past decade, many attempts have been made to estimate non-photosynthetic vegetation cover based on remotely sensed data [5–17]. Very few studies have been conducted, however, of non-photosynthetic biomass estimation based on remotely sensed data.

The reflectance spectra of both non-photosynthetic vegetation and soil lack the unique spectral signature of green vegetation in the 400–1100 nm wavelength region [5,14]. Non-photosynthetic vegetation and soil are often spectrally similar and differ only in amplitude for visible and near infrared wavelengths [8,17], making discrimination between

*Corresponding authors (email: gszhou@ibcas.ac.cn; xinshiz@yahoo.com)

soil and non-photosynthetic vegetation difficult or nearly impossible using reflectance techniques [11]. A lignocellulose absorption trough at 2100 nm in the reflectance spectra of non-photosynthetic vegetation has been observed; this may have been caused by cellulose, hemicellulose, lignin, or other structural compounds [18,19]. The absorption near 2100 nm is absent from soil or green vegetation reflectance spectra [10,17,20]. Daughtry et al. [9] defined a hyperspectral variable, called cellulose absorption index (CAI), which described the depth of the lignocellulose absorption feature in the 2000–2200 nm wavelength region.

In addition, efforts to enhance the discrimination of non-photosynthetic vegetation from soil have led to numerous spectral indices that incorporate the Landsat Thematic Mapper (TM) shortwave infrared bands, such as the normalized difference index (NDI) [14], the soil adjusted corn residue index (SACRI) [7], and the modified soil adjusted crop residue index (MSACRI) [21]. However, these broadband spectral indices were only weakly correlated to non-photosynthetic vegetation cover [12,20].

Although CAI was found effective for estimation of non-photosynthetic vegetation cover [12,13,15], the potential of CAI for estimating non-photosynthetic biomass remains to be examined. Additionally, MODIS (Moderate Resolution Imaging Spectroradiometer) data have long been the primary source in grassland surveys because of their large scale, temporal continuity, and low cost. However, the narrow wavelength ranges in CAI calculations are not available from MODIS. To achieve regional non-photosynthetic biomass estimation based on MODIS data, the biggest challenge is to find a surrogate index for CAI in MODIS surface reflectance data.

Our aim was to ascertain the utility of CAI for estimating non-photosynthetic biomass of desert steppe in Inner Mongolia. More specifically, our objectives were to (1) evaluate the effectiveness of CAI derived from hyperspectral field spectrometer (Analytical Spectral Device, ASD) measurements and a spaceborne hyperspectral sensor (Hyperion) for quantifying non-photosynthetic biomass; and (2) find a MODIS surrogate index for CAI and compare the performance of the surrogate index with TM-derived indices such as NDI, SACRI, and MSACRI, in estimating non-photosynthetic biomass.

1 Materials and methods

1.1 Study site

The experiment was conducted at Sonid Zuoqi temperate desert steppe ecosystem research station (44°05′19"N, 113°34′20"E, 972 m above sea level) (Figure 1), Inner Mongolia, China. The steppe area is characterized by cold, dry winters, and warm, humid summers. Long-term mean annual temperature is 3.1°C with monthly mean temperature ranging from −18.7°C in January to 22°C in July. Long-term mean annual precipitation is approximately 185 mm, with

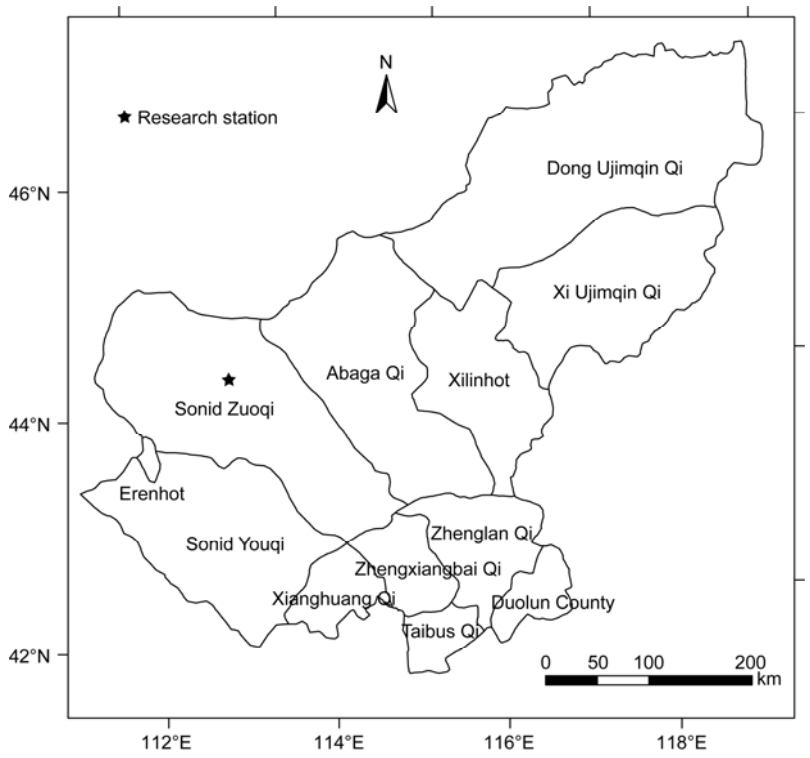

Figure 1 The location of Sonid Zuoqi temperate desert steppe ecosystem research station.

85% during the growing season (May to September). According to the Chinese Soil Classification System, the soil is brown calcic soil; equivalent to orthid and argid in the United State Soil Taxonomy [22]. The desert steppe vegetation is dominated by *Stipa klemenzii* Roshev. and the main species are *Agropyron desertorum* (Fisch.) Schult., *Cleistogenes squarrosa* (Trin.) Keng, *Artemisia frigida* Willd. Sp. Pl., and *Caragana microphylia* Lam.

1.2 Data collection

Sampling was carried out during the 2009 and 2010 growing seasons. In 2009, this was 13–17 May, 6–11 June, 11–17 July, 6–13 August, and 16–20 September. In every sampling period, 16 vegetation plots and 1 bare soil plot of 0.5 m × 0.5 m were selected, following a simple random sampling method. In 2010, sampling was undertaken on 23–30 August, and 38 vegetation plots of 0.5 m × 0.5 m were selected following a simple random sampling method. In total, 118 vegetation plots and 5 bare soil plots were selected to conduct field spectral and biophysical measurements. The distance between plots ranged from tens to hundreds of meter. All plots were located using a Global Positioning System (GPS) to avoid sampling a previously sampled area.

All canopy spectral measurements were taken on clear days with no visible cloud cover between 11:30 and 14:00 (local time), using an ASD spectrometer, FieldSpec3 Pro FR (Inc., Boulder, Colorado, USA). This spectrometer covered a range from 350 to 2500 nm. The sampling interval over the 350–1050 nm range was 1.4 nm with a spectral resolution of 3 nm. Over the 1050–2500 nm range, the sampling interval was 2 nm and the spectral resolution was between 10 and 12 nm. Results were interpolated using ASD software to produce readings every 1 nm. The sensor, with a field of view of 25°, was positioned 1.2 m above the vegetation canopy at the nadir position; allowing coverage of a circular area with a diameter about 0.5 m. Thirty replicates were made of each canopy spectral measurement. Prior to each reflectance measurement, the radiance of a white standard panel coated with BaSO4 and with a known reflectivity was recorded for normalization of the target measurements.

Standing biomass and litter on the soil surface were collected using traditional agronomic methods. All biomass was separated into live and non-photosynthetic biomass (litter and standing senesced biomass). To avoid mismatch between the field of view and the 0.5 m × 0.5 m quadrat of biomass measurements, a reference stack was placed at the centre of each measurement plot for collecting biomass after spectral measurements. The litter and standing senesced biomass were oven-dried at 65°C to a constant mass, and weighed to the nearest 0.1 g. Non-photosynthetic biomass (g m^{-2}) was determined by dividing the weight of the dried litter and standing senesced biomass by the surface area of the plot.

1.3 Data analysis

(i) Data pretreatment. To minimize noise in the measured reflectance spectra, the ASD spectrometer spectrum of each plot was averaged using ViewSpec Pro 5.6 software. The averaged reflectance for each plot was used for further analysis.

The simulated TM and MODIS reflectance of each plot were generated from the ASD spectrometer reflectance. Spectral resampling from ASD channels to simulated TM and MODIS bands was performed using the spectral resampling routine available in ENVI 4.3 software (Research Systems, Inc.). Sensor-specific spectral response functions were set for Landsat-5 TM and MODIS channels.

"Hyperion" is a hyperspectral spaceborne imaging spectrometer consisting of 242 bands ranging from 356 to 2577 nm that acquire data at approximately 10 nm intervals. The spectral response function for Hyperion channels is not currently available. Therefore, a Hyperion-specific spectral response function was simulated using a Gaussian function based on center wavelength and FWHM (full width at half maximum). The simulated Hyperion reflectance of each plot was then generated from ASD spectrometer reflectance using the Hyperion-specific spectral response function.

(ii) Data analysis. The total set of non-photosynthetic biomass data collected in 2009 and 2010 was split into the calibration data set (n=83) and validation data set (n=35) by random assignment. No saturation problem was found in the relationships between non-photosynthetic biomass and the investigated indices. Linear regression analyses were performed on the calibration data set. Empirical validation of linear regression models was carried out using the validation data set. The performance of linear regression models was compared using root mean squared error (RMSE) and relative error (RE) for validation. The RMSE and RE were determined using the following equations:

$$\mathrm{RMSE} = \sqrt{\frac{1}{n}\sum_{i=1}^{n}(y_i - y_i')^2}\ , \tag{1}$$

$$\mathrm{RE}(\%) = \frac{\mathrm{RMSE}}{\overline{y}} \times 100\ , \tag{2}$$

where y_i is the measured value of validation sample i, y_i' is the predicted value of validation sample i, $\overline{y}$ is the mean value of validation samples, and n is the number of validation samples (n = 35).

(iii) Spectral indices. CAI was determined using the following equation [9,10]:

$$\mathrm{CAI} = 0.5 \times (R_{2.0} + R_{2.2}) - R_{2.1}\ , \tag{3}$$

where for ASD spectrometer data, $R_{2.0}$, $R_{2.1}$ and $R_{2.2}$ are the mean reflectances at 2000–2050, 2080–2130 and 2190–2240 nm, respectively; for Hyperion data, $R_{2.0}$ is the mean reflectance in three bands centered at 1982, 1992 and 2002 nm, $R_{2.1}$ is the mean reflectance in three bands centered at

2103, 2113 and 2123 nm, and $R_{2.3}$ is the mean reflectance in three bands centered at 2194, 2204 and 2214 nm.

NDI, SACRI, and MSACRI were determined using the following equations [7,14,21]:

$$\mathrm{NDI} = (R_4 - R_5)/(R_4 + R_5), \quad (4)$$

$$\mathrm{SACRI} = \alpha(R_4 - R_5 - \beta)/(\alpha R_4 + R_5 - \alpha\beta), \quad (5)$$

$$\mathrm{MSACRI} = 5 \times \frac{\alpha(R_5 - \alpha R_7 - \beta)}{\alpha R_5 + R_7 - \alpha\beta}, \quad (6)$$

where R_4, R_5 and R_7 are the reflectances at TM bands 4, 5, and 7, respectively; α and β are the slope and intercept of the soil line equation, respectively. The soil line was constructed based on the simulated reflectance of TM bands 3 and 4, using five bare soil samples collected in 2009.

(iv) MODIS surrogate index selection. Seven simulated single MODIS bands (bands 1–7) and combinations of two of these with ASD-derived CAI were tested through simple and multiple linear regression models based on the calibration data set. The optimal MODIS surrogate index for ASD-derived CAI was decided based on the Pearson correlation coefficient and the multiple correlation coefficient. The three types of combinations of two bands were: the simple difference between the *i* and *j* bands (*i*–*j*), the simple ratio between the two bands (*i*/*j*), and the normalized difference between the two bands (*i*–*j*)/(*i*+*j*). The structure of the simple linear regression model was: CAI = $x + y \times \mathrm{MODIS_{VI}}$. The structure of multiple linear regression model was CAI = $x + y \times \mathrm{MODIS_{VI1}} + z \times \mathrm{MODIS_{VI2}}$.

2 Results and analysis

2.1 Performance of CAI for estimating non-photosynthetic biomass

The performance of CAI for estimating non-photosynthetic biomass is presented in Table 1. The ASD-derived CAI yielded high R^2 (0.70, P<0.001) with non-photosynthetic biomass. The RMSE and RE of the model involving the ASD-derived CAI were 14.4 g m^{-2} and 26.4%, respectively. Models based on the Hyperion-derived and ASD-derived CAI yielded similar performance for both calibration and validation. The R^2, RMSE, and RE of the model involving the Hyperion-derived CAI were 0.69 (P<0.001), 14.5 g m^{-2}, and 26.6%, respectively.

The sampled area was small compared with the pixel size of spaceborne Hyperion hyperspectral data, and atmospheric conditions also differed from plot-scale field observations. Nevertheless, we concluded that the shortwave infrared portion of the Hyperion data was sensitive to non-photosynthetic biomass change, and the hyperspectral Hyperion data had potential in monitoring regional non-photosynthetic biomass.

Several studied have shown that CAI was easily affected by green vegetation cover [11,12]. Because the shortwave infrared region is strongly affected by water content, the high moisture content of green vegetation significantly attenuated the reflectance signal from the lignocellulose absorption features near 2100 nm [23]. Daughtry et al. [11,12] found that small fractions of green vegetation in the scene had little effect on the overall linear relationship between CAI and crop residue cover, but as the fraction of green vegetation (>30%) increased, the errors for estimating crop residue cover using CAI increased. The vegetation in our study area was sparse, and green vegetation cover was less than 30%. Further research is necessary to assess the performance of the CAI for predicting non-photosynthetic biomass of grasslands with a high fraction of green vegetation.

Table 1 Performance of CAI for prediction of non-photosynthetic biomass

Spectral indices	Calibration (n=83)		Validation (n=35)	
	R^2	P	RMSE (g m^{-2})	RE (%)
ASD-derived CAI	0.70	<0.001	14.4	26.4
Hyperion-derived CAI	0.69	<0.001	14.5	26.6

2.2 Optimal MODIS surrogate index

As shown in Table 2, simple linear correlations between single MODIS bands or combinations of two MODIS bands and ASD-derived CAI were low ($|r|$<0.65). The best correlation was between the ASD-derived CAI and a NDVI-like normalized index of MODIS bands 2 and 5 with r=–0.64 (P<0.001). No single MODIS band or combination of two MODIS bands was able to provide the same information as the CAI derived from ASD hyperspectral bands.

Several combinations had high multiple correlation coefficients with the ASD-derived CAI in the multiple regression analyses, and the five best combinations are reported (Table 3). The best of those tested was a combination of normalized difference indices ($\mathrm{MODIS_2}$–$\mathrm{MODIS_5}$)/($\mathrm{MODIS_2}$+$\mathrm{MODIS_5}$) and ($\mathrm{MODIS_6}$–$\mathrm{MODIS_7}$)/($\mathrm{MODIS_6}$+$\mathrm{MODIS_7}$). The multiple correlation coefficient (r) was around 0.884 (P<0.001), indicating that this combination was able to provide approximately the same information as the ASD-derived CAI.

Table 2 The best five MODIS indices from simple linear models fitted between MODIS individual bands and combinations of two MODIS bands with ASD-derived CAI

$\mathrm{MODIS_{VI}}$	r	P
($\mathrm{MODIS_2}$–$\mathrm{MODIS_5}$)/($\mathrm{MODIS_2}$+$\mathrm{MODIS_5}$)	–0.641	<0.001
$\mathrm{MODIS_2}$/$\mathrm{MODIS_5}$	–0.636	<0.001
$\mathrm{MODIS_3}$–$\mathrm{MODIS_4}$	0.630	<0.001
($\mathrm{MODIS_2}$–$\mathrm{MODIS_6}$)/($\mathrm{MODIS_2}$+$\mathrm{MODIS_6}$)	–0.623	<0.001
$\mathrm{MODIS_2}$	–0.612	<0.001

Table 3 The best five combinations of MODIS indices from multiple linear models fitted between MODIS individual bands and combinations of two MODIS bands with ASD-derived CAI

$MODIS_{VI1}$	$MODIS_{VI2}$	*r*	*P*
$(MODIS_2–MODIS_5)/(MODIS_2+MODIS_5)$	$(MODIS_6–MODIS_7)/(MODIS_6+MODIS_7)$	0.884	<0.001
$(MODIS_2–MODIS_5)/(MODIS_2+MODIS_5)$	$MODIS_6/MODIS_7$	0.883	<0.001
$(MODIS_2–MODIS_5)/(MODIS_2+MODIS_5)$	$MODIS_6–MODIS_7$	0.864	<0.001
$MODIS_2$	$MODIS_6–MODIS_7$	0.836	<0.001
$MODIS_2$	$(MODIS_6–MODIS_7)/(MODIS_6+MODIS_7)$	0.810	<0.001

2.3 Performance of multi-band indices for estimating non-photosynthetic biomass

The performance of four multi-band indices for estimating non-photosynthetic biomass is presented in Table 4. The multiple regression model involving $(MODIS_2–MODIS_5)/(MODIS_2+MODIS_5)$ and $(MODIS_6–MODIS_7)/(MODIS_6+MODIS_7)$ showed a higher R^2 (0.61) than the TM-derived indices (NDI, SACRI and MSACRI); the latter showed an R^2 of less than 0.32. The multiple regression model also produced a lower RMSE (15.8 g m^{-2}) and RE (28.9%) than the TM-derived indices; these yielded RMSE and RE values of more than 23 g m^{-2} and 42%, respectively.

As shown in Figure 2, predicted values based on the multiple regression model involving $(MODIS_2–MODIS_5)/(MODIS_2+MODIS_5)$ and $(MODIS_6–MODIS_7)/(MODIS_6+MODIS_7)$ were distributed near the 1:1 line in the plot of observed versus predicted non-photosynthetic biomass. However, the models involving TM-derived indices overestimated low values and underestimated high values. The low values fell below the 1:1 line and the high values fell above the 1:1 line in the plot. A possible explanation was that the TM-derived indices were created based on only two components (soil and non-photosynthetic vegetation)

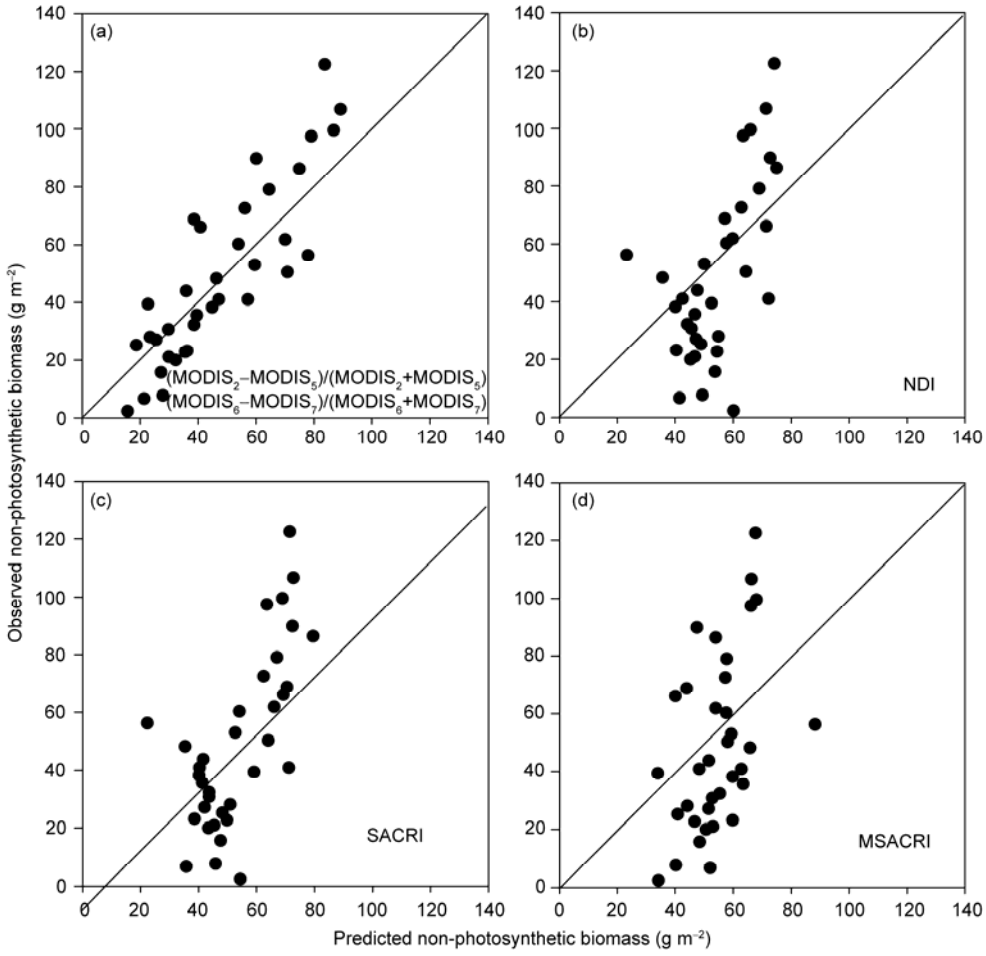

Figure 2 Observed versus predicted non-photosynthetic biomass based on four multi-band indices (the solid line corresponds to the 1:1 line).

Table 4 Performance of four multi-band indices for predicting non-photosynthetic biomass

Spectral indices	Calibration (n=83)		Validation (n=35)	
	R^2	P	RMSE (g m^{-2})	RE (%)
($MODIS_2$–$MODIS_5$)/($MODIS_2$+$MODIS_5$) ($MODIS_6$–$MODIS_7$)/($MODIS_6$+$MODIS_7$)	0.61	<0.001	15.8	28.9
NDI	0.25	<0.001	25.0	45.8
SACRI	0.31	<0.001	23.5	43.0
MSACRI	0.16	<0.001	27.3	50.0

excluding green vegetation, and were unsuitable for discriminating non-photosynthetic vegetation from green vegetation and soil.

Analysis of the above data indicated that TM-derived indices (NDI, SACRI and MSACRI) were not reliable predictors for estimating regional non-photosynthetic biomass. We suggest that MODIS data are preferable for non-photosynthetic biomass calculation when a MODIS surrogate index is found for the CAI.

3 Conclusions

We have demonstrated the utility of CAI based on hyperspectral and multispectral remotely sensed data for estimating the non-photosynthetic biomass of desert steppe in Inner Mongolia. Our main conclusions can be summarized as follows:

(1) Hyperspectral CAI, widely used for monitoring non-photosynthetic vegetation coverage, was found equally effective for non-photosynthetic biomass estimation. Regression models involving ASD-derived and Hyperion-derived CAI produced high prediction accuracy (RE=26%–27%).

(2) Although the narrow wavelength ranges in CAI calculation are not available from the MODIS sensor, the ($MODIS_2$–$MODIS_5$)/($MODIS_2$+$MODIS_5$) and ($MODIS_6$–$MODIS_7$)/($MODIS_6$+$MODIS_7$) showed a high multiple correlation with ASD-derived CAI. A predictive model based on this combination produced higher accuracy (RE=28.9%) than the previously developed TM-derived indices, such as NDI, SACRI, and MSACRI.

(3) The TM-derived NDI, SACRI, and MSACRI indices were found to be unsuitable for monitoring nonphotosynthetic biomass from a three-component mixture of green vegetation, non-photosynthetic vegetation and soil.

In addition, the Hyperion, TM, and MODIS data we used were convolved from field ASD bands based on corresponding spectral response functions. The spatial resolutions, atmospheric conditions, and observation angles of these data also differed from plot-scale, field observation. Additional research focusing on estimation of non-photosynthetic biomass from satellite and airborne remotely sensed images is thus needed to confirm our findings.

This work was supported by the National Basic Research Program of China (2010CB951303) and the National Natural Science Foundation of China (90711001 and 40971123).

1 Gao Z Q, Li J Y. Simulation study of China's net primary production. Chin Sci Bull, 2008, 53: 434–443
2 Ma W H, Fang J Y, Yang Y H, et al. Biomass carbon stocks and their changes in northern China's grasslands during 1982–2006. Sci China Ser C-Life Sci, 2010, 53: 841–850
3 Scurlock J M O, Hall D O. The global carbon sink: A grassland perspective. Glob Change Biol, 1998, 4: 229–233
4 Scurlock J M O, Johnson K, Olson R J. Estimating net primary productivity from grassland biomass dynamics measurements. Glob Change Biol, 2002, 8: 736–753
5 Aase J K, Tanaka D L. Reflectance from four wheat residue cover densities as influenced by three soil backgrounds. Agron J, 1991, 83: 753–757
6 Asner G P, Lobell D B. A biogeophysical approach for automated SWIR unmixing of soils and vegetation. Remote Sens Environ, 2000, 74: 99–112
7 Biard F, Bannari A, Bonn F. SACRI (Soil adjusted corn residue index): An index using near and mid-infrared for the detection of residues of maize (in French). In: 17th Canadian Symposium on Remote Sensing, 1995. 417–423
8 Baird F, Baret F. Crop residue estimation using multiband reflectance. Remote Sens Environ, 1997, 59: 530–536
9 Daughtry C S T, McMurtrey III J E, Nagler P L, et al. Spectral reflectance of soils and crop residues. In: Davies A M C, Williams P, eds. Near Infrared Spectroscopy: The Future Waves. Chichester: NIR Publication, 1996. 505–510
10 Daughtry C S T. Discriminating crop residues from soil by shortwave infrared reflectance. Agron J, 2001, 93: 125–131
11 Daughtry C S T, Hunt Jr E R, McMurtrey III J E. Assessing crop residue cover using shortwave infrared reflectance. Remote Sens Environ, 2004, 90: 126–134
12 Daughtry C S T, Hunt Jr E R, Doraiswamy P C, et al. Remote sensing the spatial distribution of crop residue. Agron J, 2005, 97: 864–874
13 Daughtry C S T, Doraiswamy P C, Hunt Jr E R, et al. Remote sensing of crop residue cover and soil tillage intensity. Soil Tillage Res, 2006, 91: 101–108
14 McNairn H, Protz R. Mapping corn residues cover on agricultural fields in Oxford country, Ontario, using Thematic Mapper. Can J Remote Sens, 1993, 19: 152–159
15 Nagler P L, Inoue Y, Clenn E P, et al. Cellulose absorption index (CAI) to quantify mixed soil-plant litter scenes. Remote Sens Environ, 2003, 87: 310–325
16 Smith A M, Bullock M S, Ivle C V. Estimating wheat residue cover using broad and narrow band visible-infrared reflectance. Can J Remote Sens, 2000, 26: 241–252
17 Streck N A, Rundquist D, Connot J. Estimating residue wheat dry matter from remote sensing measurements. Photogr Eng Remote Sens, 2002, 68: 1193–1201
18 Elvidge C D. Visible and near infrared reflectance characteristics of dry plant material. Int J Remote Sens, 1990, 11: 1775–1795

19 Robert D A, Smith M O, Adams J B. Green vegetation, non-photosynthetic vegetation, and soil in AVIRIS data. Remote Sens Environ, 1993, 44: 255–269
20 Cao X, Chen J, Matsushita B, et al. Developing a MODIS-based index to discriminate dead fuel from photosynthetic vegetation and soil background in the Asian steppe area. Int J Remote Sens, 2010, 31: 1589–1604
21 Bannari A, Haboudane D, Bonn F. Mid infrared interest for culture residues cartography. Can J Remote Sens, 2000, 26: 384–393
22 Gong Z T, Chen Z C, Shi X Z. Chinese Soil Taxonomy: Theory, Method, Practice (in Chinese). Beijing: Science Press, 1999. 1–903
23 Murphy R J. The effects of surficial vegetation cover on mineral absorption feature parameters. Int J Remote Sens, 1995, 16: 2153–2164